

Geophysical Research Letters[®]



RESEARCH LETTER

10.1029/2023GL106695

Inferring Whistler-Mode Chorus Wave Source Regions in the Martian Mini-Magnetospheres

Sanwei Cheng^{1,2,3} , Zhenpeng Su^{1,2,3} , Zhiyong Wu^{1,2,3} , and Yuming Wang^{1,2,3} 

¹Deep Space Exploration Laboratory/School of Earth and Space Sciences, University of Science and Technology of China, Hefei, China, ²CAS Center for Excellence in Comparative Planetology/CAS Key Laboratory of Geospace Environment/Mengcheng National Geophysical Observatory, University of Science and Technology of China, Hefei, China, ³Collaborative Innovation Center of Astronautical Science and Technology, Harbin, China

Key Points:

- Chorus wave sources are located by matching the frequency dependence between the modeled linear growth rates and the observed power
- Martian mini-magnetospheres contain continuous or intermittent wave sources spanning up to 40% of the entire magnetic field line length
- Martian mini-magnetospheres could have more active energy transfer processes mediated by chorus than the expectation

Supporting Information:

Supporting Information may be found in the online version of this article.

Correspondence to:

Z. Su,
szpe@mail.ustc.edu.cn

Citation:

Cheng, S., Su, Z., Wu, Z., & Wang, Y. (2024). Inferring whistler-mode chorus wave source regions in the Martian mini-magnetospheres. *Geophysical Research Letters*, 51, e2023GL106695. <https://doi.org/10.1029/2023GL106695>

Received 7 OCT 2023

Accepted 12 JAN 2024

Abstract Martian mini-magnetospheres contain whistler-mode chorus waves potentially contributing to atmospheric escape, analogous to the Earth's inner magnetosphere. At Earth, the chorus waves have been found to originate from the near-equatorial region spanning approximately 2% of the entire magnetic field line length. However, because of the lack of wave Poynting flux measurements, the Martian chorus source region remains unclear. By comparing the frequency dependence between observed wave power and modeled linear growth rates, we present the first attempt to explore the chorus wave source distribution along the Martian mini-magnetospheric field lines. Our data-to-model comparisons support that these waves are not generated by a single source tightly confined near the magnetic strength minimal location but by intermittent or continuous sources spanning up to 40% of the entire field line length. These results imply that the Martian mini-magnetospheres could have more active energy transfer processes mediated by whistler-mode chorus waves than the expectation.

Plain Language Summary Atmospheric escape is a critical process for the evolution of the surface habitability of terrestrial planets in our solar system or beyond. Analogous to the Earth's inner magnetosphere, the Martian mini-magnetospheres formed by crustal magnetic fields contain whistler-mode chorus waves which have the potential to contribute to atmospheric escape. However, because of the lack of wave Poynting flux measurements, where the Martian chorus waves are generated remains unclear. By comparing the frequency dependence between the observed wave power spectral densities and the modeled linear growth rates, we present the first attempt to explore the distribution of chorus wave sources along the magnetic field lines of the Martian mini-magnetospheres. We show that these Martian chorus waves are generated by intermittent or continuous sources spanning up to 40% of the entire magnetic field line length, in contrast to the Earth's inner magnetospheric chorus waves with a single near-equatorial source spanning approximately 2% of the entire field line length. These results imply that the Martian mini-magnetospheres could have more active energy transfer processes mediated by whistler-mode chorus waves than the expectation from analogy to the Earth's magnetosphere.

1. Introduction

Atmospheric escape is a critical process for the evolution of the surface habitability of terrestrial planets in our solar system or beyond (e.g., Dong et al., 2020; Gronoff et al., 2020; Owen, 2019; Tian, 2015). In essence, the ionized or neutral atmospheric particles that are able to escape into interplanetary space must have gained enough energy to overcome the planetary gravitational potential. As a common way to exchange energy in space and astrophysical plasma, wave-particle interactions have been recognized as important procedures for planetary atmospheric escape (e.g., Ergun et al., 2006; Espley et al., 2004; Fowler et al., 2018; Gronoff et al., 2020; Jarvinen et al., 2020; Strangeway et al., 2005; Su et al., 2020).

In the case of Earth, one of the important plasma wave types contributing to atmospheric escape is the whistler-mode chorus (e.g., Newell et al., 2009; Seki et al., 2001; Thorne et al., 2010). The chorus waves occur frequently in the Earth's inner magnetosphere (e.g., Burtis & Helliwell, 1969; Horne et al., 2013; Li et al., 2009; Meredith et al., 2001) and typically appear as a succession of rising tones over the frequency range of 0.05–0.8 electron gyrofrequency in the frequency-time spectrogram (e.g., Santolík et al., 2014; Tsurutani & Smith, 1977). Through the cyclotron resonant scattering, the chorus waves precipitate the magnetospheric electrons with energies of

© 2024. The Authors.

This is an open access article under the terms of the [Creative Commons Attribution-NonCommercial-NoDerivs License](https://creativecommons.org/licenses/by/4.0/), which permits use and distribution in any medium, provided the original work is properly cited, the use is non-commercial and no modifications or adaptations are made.

0.1–10 keV into the atmosphere and then produce the diffuse aurora (e.g., Horne et al., 2003; Ni et al., 2008; Thorne et al., 2010). As the dominant energy source for the high-latitude ionosphere, the diffuse auroral precipitation eventually facilitates the ionospheric ion outflows (Newell et al., 2009), which is one of the important atmospheric escape routes (Seki et al., 2001). Different from Earth, Mars lacks a global magnetic field to shield itself from the solar wind. However, the crustal magnetic fields at Mars can form the mini-magnetospheres extending up to altitudes of 500 km (Krymskii et al., 2003). There have been observations showing the existence of whistler-mode waves with rising-tone frequency-time structures in the Martian mini-magnetospheres (Harada et al., 2016), which are further interpreted as chorus waves in a recent particle simulation (Teng et al., 2023). Some quasi-linear calculations (A. Shane & Liemohn, 2021; A. D. Shane & Liemohn, 2022) have shown the ability of whistler waves to scatter electrons in the Martian mini-magnetospheres.

Where a specific plasma wave is generated is a fundamental question that informs the quantification of its effect on the atmospheric escape. In the Earth's inner magnetosphere, both theoretical analysis and measurements of wave Poynting fluxes have demonstrated the single chorus source around the magnetic equator (Helliwell, 1969, 2014; LeDocq et al., 1998; Santolík et al., 2004; Teng et al., 2018). With the conservation of the magnetic moment invariant, the hot electron temperature anisotropy peaks at the equator (i.e., the magnetic strength minimal location). At the same location, the magnetic field inhomogeneity minimizes (Helliwell, 1969; Katoh & Omura, 2013; LeDocq et al., 1998; Omura et al., 2008). The two factors facilitate the generation of whistler-mode chorus waves from the linear and nonlinear cyclotron instabilities of hot electrons near the equator (Omura et al., 2008). These waves are not confined near the equator but propagate over a broad range approximately along the magnetic field lines (Bortnik et al., 2006; Horne et al., 2003). By analogy, in the Martian mini-magnetospheres, the generation of chorus waves has been attributed to the temperature anisotropy instabilities of hot electrons (Harada et al., 2016; Teng et al., 2023). Harada et al. (2016) calculated the local linear growth rates of waves. Most of the time, the local linear growth rates appeared to be able to explain the peak frequency of observed waves. Teng et al. (2023) modeled the nonlinear growth of waves near the magnetic strength minimal location which was selected mainly from analogy to the Earth's magnetosphere. However, because of the lack of wave Poynting flux measurements, the source region of chorus waves has not been experimentally delimited yet.

Inspired by the finding that the power spectral densities of whistler-mode waves exhibit an analogous frequency dependence to the linear growth rates at the source region in the Earth's inner magnetosphere (e.g., Su et al., 2014, 2018), we here present the first attempt to explore the chorus wave source distribution along the Martian mini-magnetospheric field lines by the frequency-dependence matching. We show that the Martian chorus waves are not generated by a single source tightly confined near the magnetic strength minimal location but by sources distributed intermittently or continuously over a broad range of the magnetic field lines. The Martian mini-magnetospheres could have more active energy transfer processes mediated by whistler-mode chorus waves than the expectation from analogy to the Earth's magnetosphere.

2. Event Overview

We revisit the 12 July 2015 event reported early by Harada et al. (2016). The Mars Atmosphere and Volatile EvolutionN (MAVEN) (Jakosky et al., 2015) spacecraft was orbiting Mars with an apoapsis altitude of ~6,000 km and a periapsis altitude of ~120 km (Figure 1a). At the low-altitude (300–500 km) southern hemisphere of Mars from 05:59:00 UT to 06:04:00 UT (Figure 1b), the magnetometer (MAG) (Connerney et al., 2015) measured the strong (up to 80 nT) magnetic fields \mathbf{B} which can be approximately decomposed as

$$\mathbf{B} \approx \mathbf{B}_{cs} + \mathbf{B}_{sw} \quad (1)$$

with the crustal field \mathbf{B}_{cs} modeled by J. W. Gao et al. (2021) and the estimated piled-up solar wind magnetic field $\mathbf{B}_{sw} = (0, 0, 13)$ nT in the Mars-centered Solar Orbital coordinate system. Given these magnetospheric measurements were made near the equator on the dawnside and the solar wind was observed to have the magnetic fields approximately along the z -direction at the nearest moment (Figure 1a), the estimation of the piled-up field \mathbf{B}_{sw} is reasonable. Without direct sunlight, the background electron density (Figure 1c) provided by the Langmuir Probe and Waves (LPW) instrument (Andersson et al., 2015) fluctuated below 350 km, consistent with previous measurements (Duru et al., 2011; Gurnett et al., 2010). On Mars, photoelectrons are mainly produced by the ionization of CO_2 on the top of the atmosphere and peak in the energy range of 20–30 eV (Frahm et al., 2006; Mantas & Hanson, 1979). As measured by the solar wind electron analyzer (SWEA) (Mitchell et al., 2016), the parallel

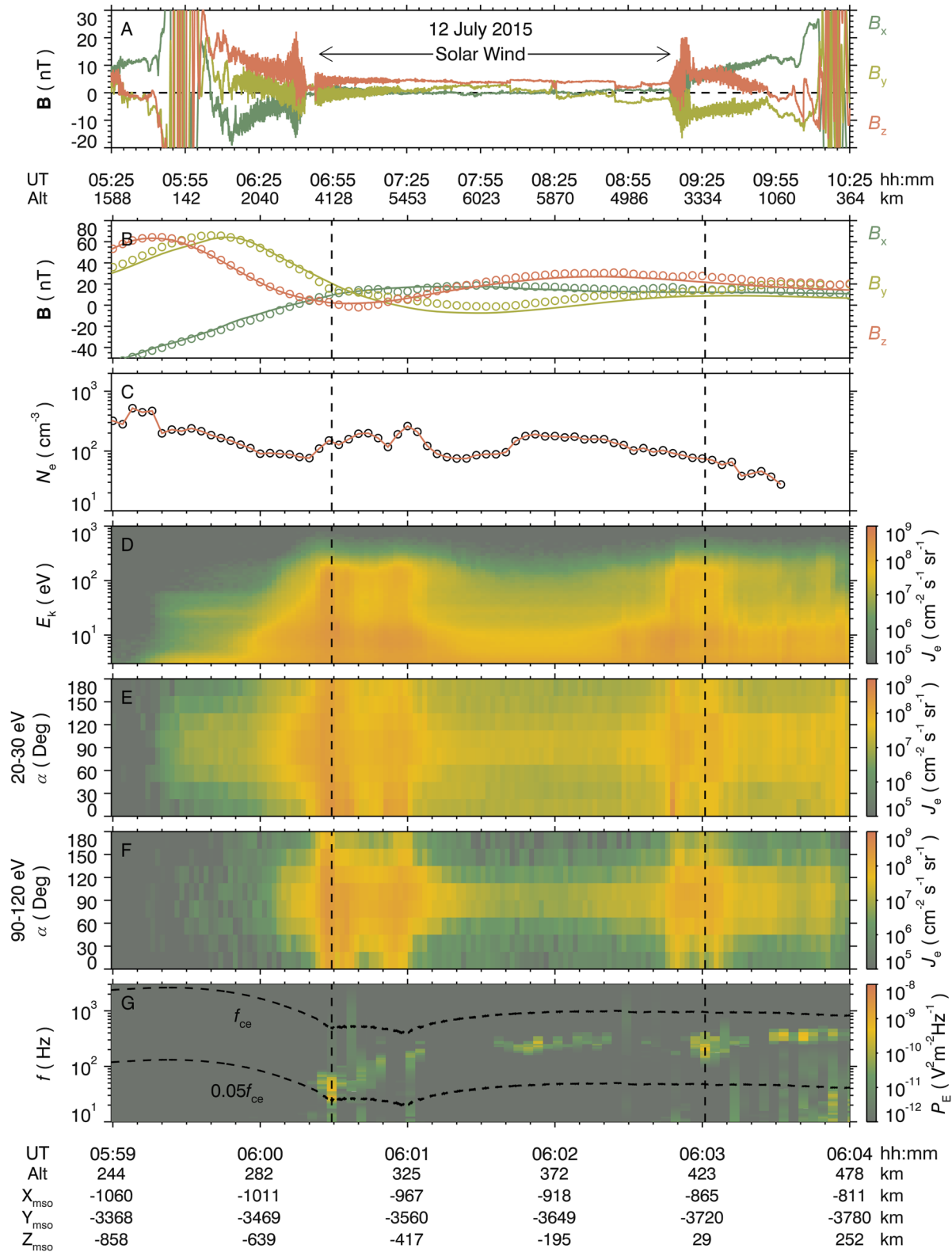


Figure 1. An event overview of whistler-mode chorus waves in the Martian mini-magnetospheres. (a) Magnetic fields $\mathbf{B} = (B_x, B_y, B_z)$ in the Mars-centered Solar Orbital (MSO) coordinate system observed within approximately one orbital period. (b) Zoom-in observed (circles) and modeled (lines) magnetic fields \mathbf{B} within 5 min in the MSO coordinate system. (c) Observed (circles) electron density N_e , whose altitudinal dependence is described by a cubic spline (line). (d) Omnidirectional electron differential energy flux J_e (color-coded). (e) Pitch-angle-dependent electron differential energy flux J_e in the energy ranges of 20–30 eV (e) and 90–120 eV (f). (g) Wave electric power spectral density P_E , overlain by two dashed lines marking frequencies of $0.05f_{ce}$ and f_{ce} .

and antiparallel 20–120 eV electron fluxes were at an extremely low level most of the time (Figures 1d–1f), indicating that both foot points of the magnetic field lines were in the nightside ionosphere (Xu et al., 2017). Around 06:00:30 UT and 06:02:50 UT, there were injections of solar wind electrons with energies approximately from 10 to 500 eV (Figure 1d). These injected 90–120 eV electrons generally peaked at the 90° pitch-angle and exhibited the two-sided loss-cones (Figure 1f). The corresponding 20–30 eV electrons exhibited the bidirectional source cones (Figure 1e), which may be a result of the additional ionization by solar wind electron precipitation at both foot points of the magnetic field lines in the nightside ionosphere (Cao et al., 2021; Lillis & Fang, 2015). All these characteristics of magnetic fields and electrons support that MAVEN was inside the Martian mini-magnetospheres. In these mini-magnetospheres, intense waves were detected by LPW (Andersson et al., 2015) in the frequency range of 0.05–0.5 f_{ce} (f_{ce} is the local electron gyrofrequency). As shown by Harada et al. (2016), these waves exhibited discrete rising tones in the high-resolution frequency-time spectrograms. Therefore, these waves could be identified as the whistler-mode chorus waves (Teng et al., 2023).

3. Whistler-Electron Cyclotron Resonance

The non-relativistic linear cyclotron resonant condition can be written as

$$\omega - k_{\parallel}v_{\parallel} = -n|\Omega_{ce}| \quad (2)$$

with the wave angular frequency $\omega = 2\pi f$, wave parallel vector $k_{\parallel} = k\cos\psi$, wave normal angle ψ , electron angular gyrofrequency $|\Omega_{ce}| = 2\pi f_{ce}$, electron parallel velocity $v_{\parallel} = v\cos\alpha$, and electron pitch-angle α . The growth of whistler-mode waves usually peaks at $\psi = 0^\circ$ through the fundamental resonance $n = -1$ (Omura et al., 2008). As indicated in Texts S1 and S2 and Figures S1–S4 in Supporting Information S1, the oblique whistler waves could experience significant Landau damping (Bortnik et al., 2006; Xiao, 2006; Xiao et al., 1998). For a given parallel-propagating wave, the resonant electrons with $\alpha = 0^\circ$ have the minimum energy (Summers et al., 2007a, 2007b)

$$E_{\min} = \frac{1}{2}m_e v_{\parallel}^2 = \frac{1}{2}m_e \left(\frac{\omega - |\Omega_{ce}|}{k} \right)^2 = \frac{1}{2}m_e c^2 \left(\frac{\omega/|\Omega_{ce}| - 1}{kc/|\Omega_{ce}|} \right)^2. \quad (3)$$

We assume the typical ion composition 40%O⁺ + 60%O₂⁺ (A. Shane & Liemohn, 2021; Su et al., 2020), determine the wavevector from the cold plasma wave dispersion relation, and obtain the minimum resonant energy E_{\min} dependent on the dimensionless wave frequency ff_{ce} and electron plasma frequency f_{pe}/f_{ce} (Figure 2). Note that for the whistler-mode chorus waves of interest, their dispersion relations are insensitive to the ion compositions. It is found that both the wavelength λ and the minimum resonant energy E_{\min} are negatively correlated to ff_{ce} and f_{pe}/f_{ce} . For the source electrons in a given energy range, the excited whistler-mode waves have lower ff_{ce} values in the region with higher f_{pe}/f_{ce} values. For the 12 July 2015 event with $ff_{ce} = 0.05 - 0.5$ and $f_{pe}/f_{ce} = 220 - 80$ (black dots in Figure 2), the wavelength λ ranged from 0.05 $c/|\Omega_{ce}|$ to 0.2 $c/|\Omega_{ce}|$ (i.e., 5–20 km). The corresponding electron minimum resonant energy was roughly several tens of eV (Figure 2c), indicating that the whistler-mode chorus waves were mainly excited by the high-energy electrons of solar wind origin.

4. Linear Growth of Whistler-Mode Waves

To infer the source region of chorus waves in the Martian mini-magnetospheres, we calculate the growth rates of whistler-mode waves along the magnetic field lines using the previously developed code (Liu et al., 2018a, 2018b; Su et al., 2018) on the basis of the linear instability theory (Chen et al., 2010; Kennel & Petschek, 1966). To avoid repetition and facilitate readers, we give the detailed expression of the linear growth rate in Text S1 in Supporting Information S1. We make the specific calculations for two moments 06:00:29 UT and 06:03:01 UT with the peaked wave power (Figure 1g). There are three inputs to our code: (a) cold electron density, (b) background magnetic field strength, and (c) hot electron phase space density (approximately from 3 to 250 eV). As shown in Figure 1c, MAVEN had moved <0.4 hr of local time within 5 min. We assume that in the spatial region without direct sunlight, the cold electron density (Figure 1c) depends on only the altitude. We assume the magnetic field strength

$$|\mathbf{B}| = r_0|\mathbf{B}_{cs} + \mathbf{B}_{sw}| \quad (4)$$

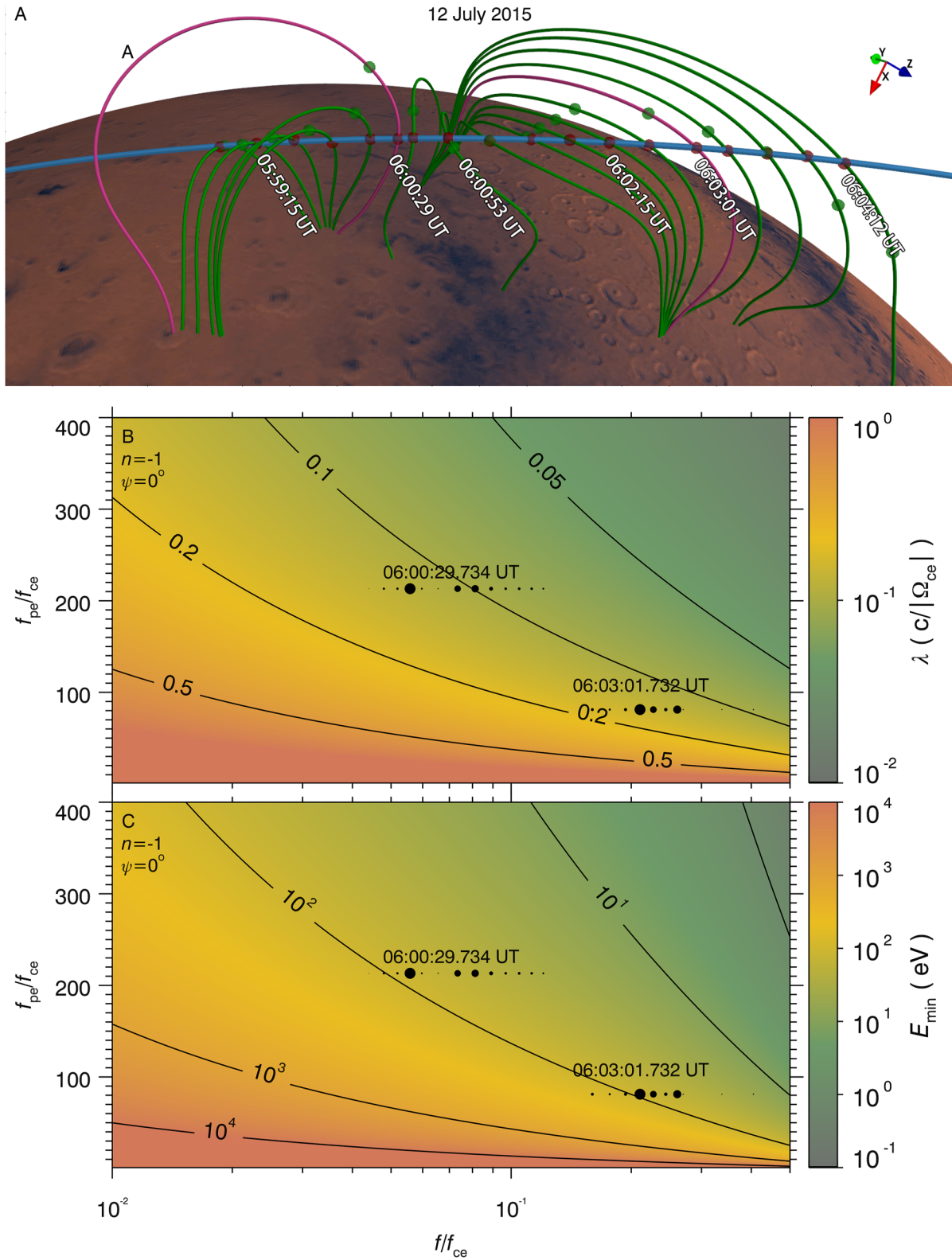


Figure 2.

with the scale factor r_0 (~ 0.82 at 06:00:29 UT and ~ 1.3 at 06:03:01 UT) determined from the local measurements. This scaling aims to match exactly the observed magnetic strengths at the two moments and does not affect the global magnetic field configuration. With the conservation of magnetic moment, we map the observed electron phase space density along the entire field line. At each location, we use the smooth cubic splines to approximate the electron phase space densities. We introduce the magnetic field line length S , which equals 0 at the sampling location of MAVEN and takes a positive value in the direction parallel to the magnetic field vector and a negative value in the antiparallel direction. To allow the wave to propagate to the observer, the wave normal angle ψ is set to be 180° when $S > 0$ and 0° when $S < 0$.

For the 06:00:29 UT moment, the modeled magnetic field line of $\sim 1,530$ km length is dipolar-like (Figure 2a). At the observer location, the modeled magnetic field vector is approximately perpendicular to the Martian surface (with an angle of 79°), consistent with the observation. From the observer to the magnetic minimal location ($S = -158$ km), the magnetic strength decreases from 18.25 to 9.46 nT (Figure 3a). When the observed hot electron phase space density (Figure 3b) is adiabatically mapped to the magnetic minimal location (Figure 3c), a “gap” emerges around the 90° pitch-angle. The modeled linear growth rate at the observer location has a comparable frequency dependence with the observed wave power (Figure 3d). Even slightly away from the observer, the frequency-dependence pattern of the linear growth rate varies significantly (Figure 3f). Particularly, at the magnetic minimal location (Figure 3e), because of the changes in both magnetic strength and density, the modeled linear growth rate peaks at 15 Hz, approximately 25 Hz away from the central frequency of observed waves. These results support that the observed strong waves were excited locally (~ 158 km away from the magnetic minimal location). The available measurements cannot help address whether the other regions, such as the magnetic minimal location, were able to produce waves. Because of the variation in the hot electron temperature anisotropy, the observer location has a smaller linear growth rate than the magnetic minimal location. Meanwhile, compared to the observer location, the magnetic minimal location has a smaller magnetic field inhomogeneity $\frac{1}{B} \frac{\partial^2 B}{\partial S^2}$ (Katoh & Omura, 2013; Omura et al., 2008) and then a lower threshold amplitude for the nonlinear growth of waves. Therefore, the magnetic minimal location has a greater potential to produce waves. The present observations of locally generated waves, in turn, imply that there could be multiple sources for chorus waves along the field line. Along the field line, there were drastic density fluctuations on a scale of 10 km, comparable to or less than the whistler wavelengths (Figure 2b). According to previous simulations (e.g., Wu et al., 1996), the incident whistler waves would undergo significant reflection and refraction at these density interfaces. The field-aligned density fluctuations could have largely suppressed the long-distance propagation of waves from other sources to the observer. It should be noted that there were weak signals recorded below 30 Hz, which seemingly correspond to the wave growth at the magnetic minimal location (Figures 3e and 3f). However, we cannot determine whether these weak signals were the sporadic, damped waves from the magnetic minimal location or just some noises occurring coincidentally.

For the 06:03:01 UT moment, the modeled magnetic field line of $\sim 1,458$ km length has a relatively flat top (Figure 2a). At the observer location, the modeled magnetic field vector is roughly tangential to the Mars surface (with an angle of 24°), generally consistent with the observation of 30° angle once again. The magnetic strength, as well as the magnetic field inhomogeneity, vary little over a long distance from $S = -500$ to 100 km (Figure 4a). This quasi-uniform field zone covers both the observer location ($S = 0$) and the magnetic minimal location ($S = -106$ km). The corresponding hot electron phase space density F (Figures 4b and 4c) obtained by the adiabatic mapping is nearly constant. Both from the perspectives of linear and nonlinear instability theories, all the positions inside the quasi-uniform field zone have nearly equal potential to produce waves. Compared to the 06:00:29 UT moment (Figures 3d and 3e), the 06:03:01 UT moment (Figures 4d and 4e) has lower f_{pe}/f_{ce} values (Figure 4a) and then allows waves to grow at higher frequencies (Figure 2). As shown in Figure 4f, the modeled linear growth rates of the entire quasi-uniform field zone peak in the frequency range of 100–400 Hz where the strong waves were recorded. Specifically, the linear growth of waves near the observer (-40 km $< S < 100$ km) explains the peak frequency ~ 200 Hz of the wave power (Figure 4d), and the linear growth away from the

Figure 2. Cyclotron resonant interaction between whistler waves and electrons in the Martian mini-magnetospheres. (a) Three-dimensional configuration of magnetic field lines (green and magenta lines) and spacecraft trajectory (blue line) in the Mars-centered geographic coordinate system. The magenta lines are the magnetic field lines of interest. The red dots mark the intersections between the magnetic field lines and the spacecraft trajectory. The green dots mark the derived magnetic strength minimal locations. (b) Wavelength λ in unit of c/Ω_{ce} and (c) electron minimum resonant energy E_{min} in unit of eV for the parallel-propagating ($\psi = 0^\circ$) whistler-mode waves. Both λ and E_{min} are color-coded and dependent on the dimensionless wave frequency f/f_{ce} and electron plasma frequency f_{pe}/f_{ce} . Black dots represent the local situations at 06:00:29 UT and 06:03:01 UT, with the sizes coded according to the electric power spectral densities.

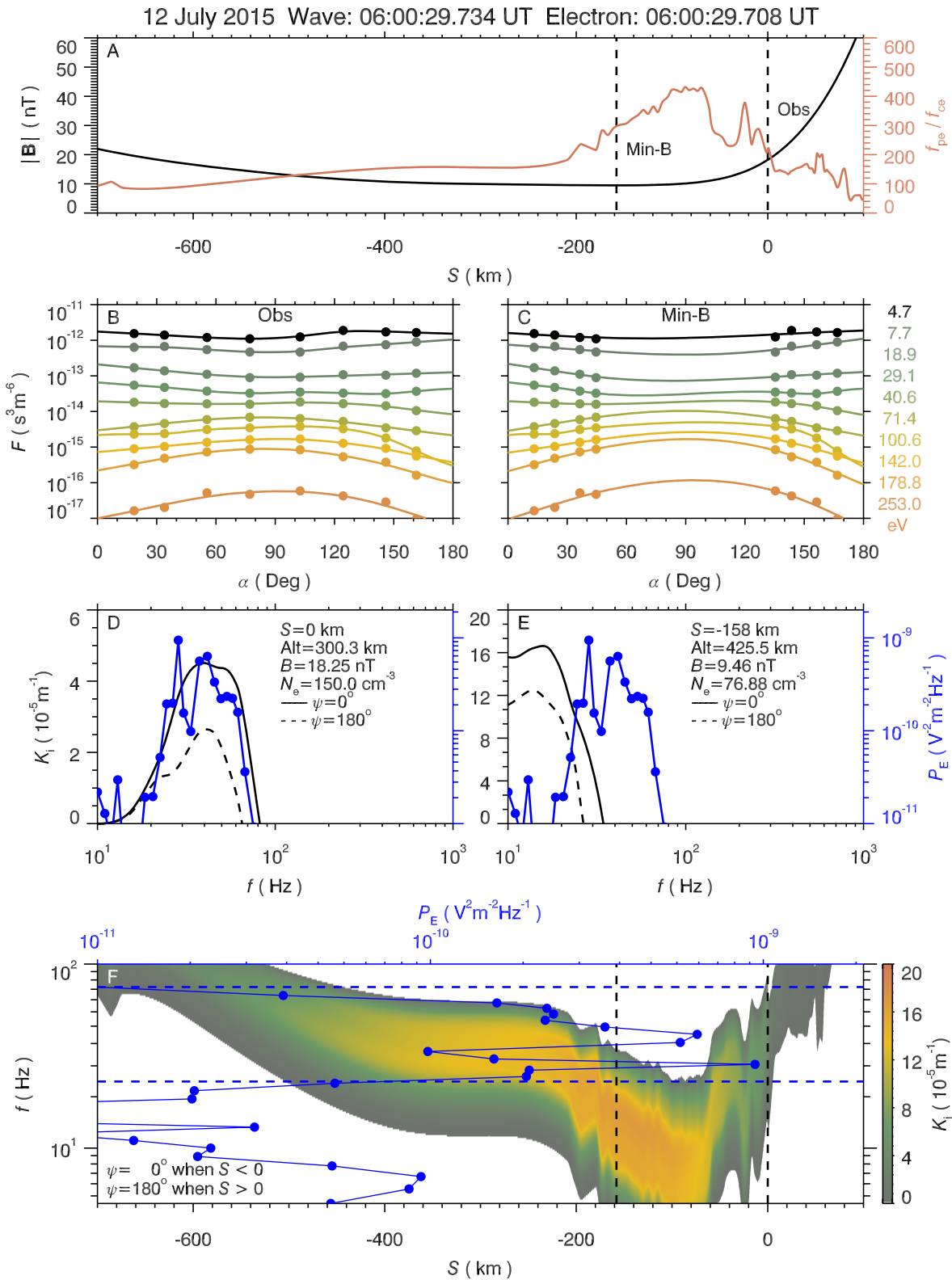


Figure 3.

observer ($-500 \text{ km} < S < -40 \text{ km}$) explains the plateau frequency 250–400 Hz of the observed wave power (Figure 4c). This frequency shift is mainly caused by the background density variation (Figure 4a). Probably because of the damping of waves during long-distance propagation, the observed wave power spectral density was higher at 200 Hz than at 250–400 Hz.

5. Conclusion and Discussion

By comparing the frequency dependence between observed power spectral densities and modeled linear growth rates, we infer that the Martian mini-magnetospheric chorus waves are not generated by a single source tightly confined near the magnetic strength minimal location but by sources distributed intermittently or continuously over a broad range of the magnetic field lines:

1. In a dipolar-like mini-magnetosphere, the linear growth process confined near the observer is appropriate to explain the central frequency and frequency coverage of the observed wave power spectral density. Approximately $\sim 158 \text{ km}$ ($\sim 10\%$ of the magnetic field line length) away from the observer, the magnetic strength minimal location has a greater potential to produce waves albeit at frequencies different from observations. The drastic oscillations of background density could have largely suppressed the propagation of waves from distant sources to the observer.
2. In a flat-top mini-magnetosphere, the linear growth process over a 550 km long distance along the field line is required to explain the peak frequency and high-frequency plateau of the observed wave power spectral density near the magnetic strength minimal location. The inferred sources for the observed waves are continuously distributed in the region with the quasi-uniform magnetic field and the smoothly behaving background electron density, where the long-distance propagation of waves is favored. This segment with the inferred sources accounts for $\sim 40\%$ of the length of the entire magnetic field line above the Martian surface.

The peak linear convective growth rate of chorus waves in the Martian mini-magnetospheres is approximately 10^{-5} m^{-1} , two orders of magnitude higher than that in the Earth's inner magnetosphere (Jin et al., 2022; Omura, 2021; Su et al., 2018). When the waves grow linearly to a sufficiently high level, the nonlinear processes take place. The nonlinear growth rate could be one order of magnitude higher than the linear one at both Mars and Earth (Omura, 2021). The peak instantaneous amplitudes of chorus waveforms are on the order of 1 nT at both Mars and Earth (Z. Gao et al., 2018; Santolík et al., 2014; Teng et al., 2023). At Earth, the effective amplification of waves takes place within a 1,000 km long distance (e.g., Omura et al., 2008; Santolík et al., 2004), $\sim 2\%$ of the field line length. At Mars, a 10 km long distance, $\sim 1\%$ of the field line length, is sufficient for the wave amplification, as supported by a recent particle simulation (Teng et al., 2023). Compared to the prediction of linear growth theory, the nonlinear amplification processes would cause the wave band to smoothly extend to higher frequencies but would not significantly change the peak frequency of wave band nor produce an additional power plateau at a certain wave band (Omura, 2021). Therefore, a combination of linear and nonlinear instabilities may not qualitatively change our conclusion.

Different from the Earth's inner magnetosphere with a relatively smooth field-aligned density profile, the Martian nightside mini-magnetospheres contain wavelength-scale density fluctuations along the magnetic field lines. In the one-dimensional particle simulation of Teng et al. (2023) at 06:00:53 UT on 12 July 2015, the observation point was quite close to the magnetic strength minimal location (Figure 2a). Their modeling well reproduced the rising tone characteristics of locally observed chorus waves. However, their simulation had a limited computational domain of $\sim 200 \text{ km}$ and assumed a constant density. More realistic particle simulations are still required to understand the generation and propagation of whistler-mode chorus waves in the Martian nightside mini-magnetospheres.

As shown by the previous statistical survey of Harada et al. (2016), the narrowband whistler-mode waves near the Martian strong crustal fields are not rare. The wave events of Figures 3 and 4 were observed at the close time

Figure 3. Locating wave sources in a dipolar-like mini-magnetosphere. (a) Magnetic field strength $|B|$ (black line) and dimensionless plasma frequency f_{pe}/f_{ce} (tawny line) dependent on the length of the magnetic field line S , with two vertical dashed lines marking the observer location and the magnetic strength minimal location. In the following two columns, the left panels (b and d) are for the observer location and the right panels (c and e) are for the magnetic strength minimal location. (b and c) Observed (dots) and modeled (lines) pitch-angle-dependent electron phase space densities F . Colors help differentiate among the energy channels which have been corrected according to the spacecraft potential. (d and e) Linear convective growth rates K_i of parallel (solid lines) and antiparallel (dashed lines) whistler-mode waves, in comparison to the observed wave electric power spectral densities P_E (blue dots, with the solid lines to guide the eye). (f) Linear convective growth rate K_i (color-coded) over the entire field line, with the normal angle $\psi = 0^\circ$ when $S < 0$ and $\psi = 180^\circ$ when $S > 0$.

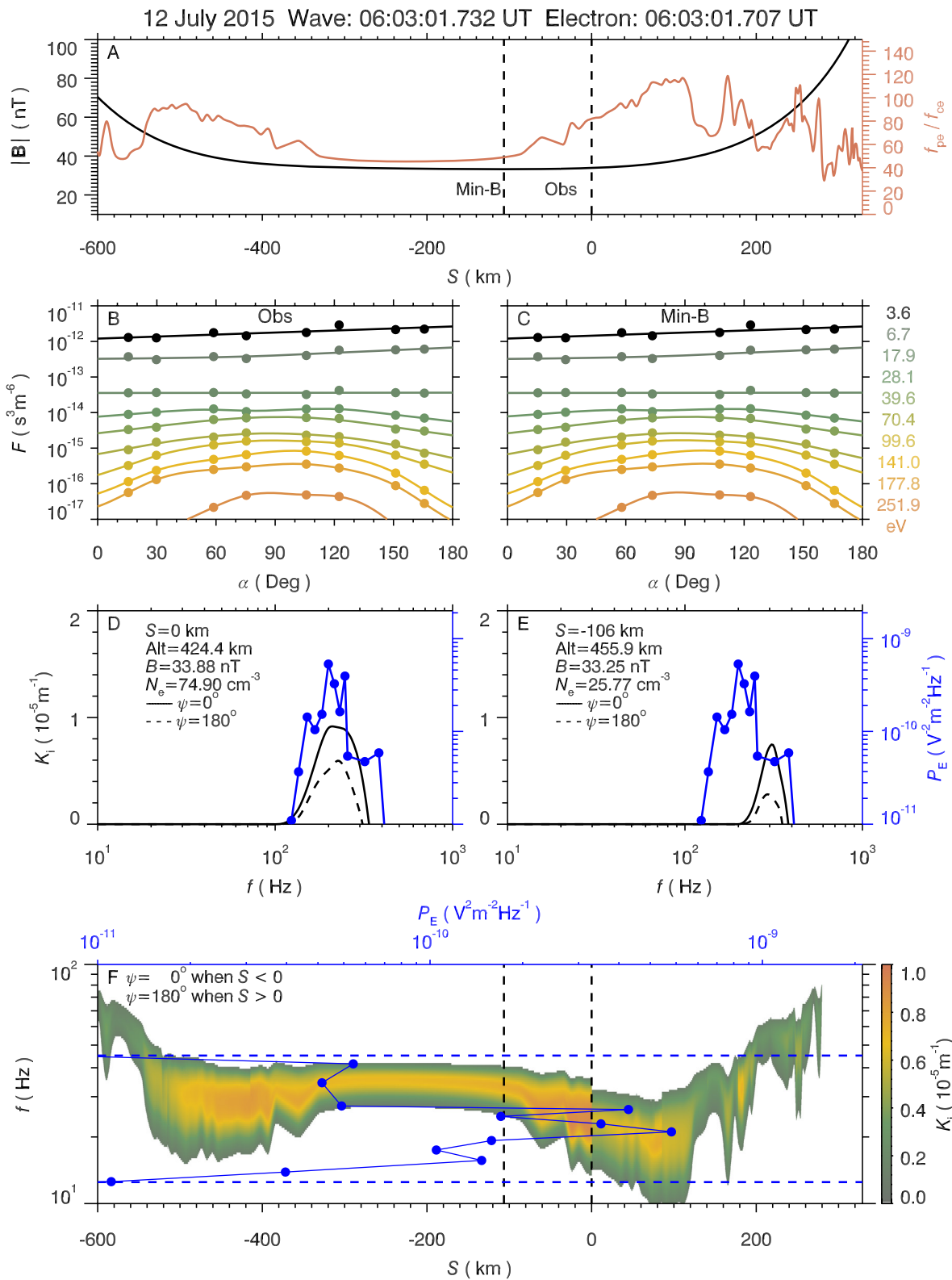


Figure 4. Locating wave sources in a flat-top mini-magnetosphere, with the same format as Figure 3.

moments but in the different mini-magnetospheres (Figure 2a). We have analyzed another two wave events on the dipolar-like magnetic field lines at different time periods in the Supporting Information (Figures S5–S10 in Supporting Information S1). For the event at 08:25:48 UT on 19 July 2015, the magnetic field line had a length of 888 km and the observer was quite close to the magnetic strength minimal location, similar to the situation of Teng et al. (2023). For the event at 01:28:50 UT on 18 July 2015, the magnetic field line had a length of 2,484 km and the observer was 466.7 km away from the magnetic strength minimal location. For both events (Figures S6–S10 in Supporting Information S1), the linear growth process near the observer is appropriate to explain the central frequency and frequency coverage of the observed wave power spectral density. The four events in the main text and Supporting Information S1 were scattered over a range of 27° latitude and 52° longitude in the Mars-centered geographic coordinate system. These results support the generality of our conclusion.

Our results imply that the Martian mini-magnetospheres could have more active energy transfer processes mediated by whistler-mode chorus waves than the expectation from analogy to the Earth's magnetosphere. We reiterate that the present study is limited by the single-point observations and by the absence of wave Poynting flux measurements. In future Mars missions, more comprehensive measurements are required to examine the present inference.

Data Availability Statement

Mars Atmosphere and Volatile Evolution Data used in the study is available on NASA Planetary Data System (2023). We analyzed the following data: (a) L2 MAG data (Connerney, 2023), (b) L2 LPW data (Andersson, 2023), (c) L2 SWEA data (Mitchell, 2023), and (d) MAVEN In Situ Key Parameters (Dunn, 2023).

Acknowledgments

We acknowledge the entire MAVEN team for providing data. This work was supported by the National Natural Science Foundation of China Grants 42130204, 42188101, 42274198, and 42074222, the Strategic Priority Research Program of Chinese Academy of Sciences Grant XDB 41000000, and the Key Research Program of the Chinese Academy of Sciences Grant ZDRE-KT-2021-3.

References

- Andersson, L. (2023). MAVEN LPW calibrated data bundle [Dataset]. NASA Planetary Data System. Retrieved from <https://pds-ppi.igpp.ucla.edu/search/view/?f=yes&id=pds://PPI/maven.lpw.calibrated>
- Andersson, L., Ergun, R. E., Delory, G. T., Eriksson, A., Westfall, J., Reed, H., et al. (2015). The Langmuir Probe and Waves (LPW) instrument for MAVEN. *Space Science Reviews*, 195(1–4), 173–198. <https://doi.org/10.1007/s11214-015-0194-3>
- Bortnik, J., Inan, U. S., & Bell, T. F. (2006). Landau damping and resultant unidirectional propagation of chorus waves. *Geophysical Research Letters*, 33(3), L03102. <https://doi.org/10.1029/2005GL024553>
- Burtis, W. J., & Helliwell, R. A. (1969). Banded chorus—A new type of VLF radiation observed in the magnetosphere by OGO 1 and OGO 3. *Journal of Geophysical Research*, 74(11), 3002–3010. <https://doi.org/10.1029/JA074i011p03002>
- Cao, Y. T., Cui, J., Wu, X. S., Niu, D. D., Lai, H. R., Ni, B. B., et al. (2021). A survey of photoelectrons on the nightside of Mars. *Geophysical Research Letters*, 48(2), e89998. <https://doi.org/10.1029/2020GL089998>
- Chen, L., Thorne, R. M., Jordanova, V. K., & Horne, R. B. (2010). Global simulation of magnetosonic wave instability in the storm time magnetosphere. *Journal of Geophysical Research*, 115(A11), A11222. <https://doi.org/10.1029/2010JA015707>
- Connerney, J. E. P. (2023). MAVEN MAG calibrated data bundle [Dataset]. NASA Planetary Data System. <https://doi.org/10.17189/1414178>
- Connerney, J. E. P., Espley, J., Lawton, P., Murphy, S., Odom, J., Oliverson, R., & Sheppard, D. (2015). The MAVEN magnetic field investigation. *Space Science Reviews*, 195(1–4), 257–291. <https://doi.org/10.1007/s11214-015-0169-4>
- Dong, C., Jin, M., & Lingam, M. (2020). Atmospheric escape from TOI-700 d: Venus versus Earth analogs. *The Astrophysical Journal Letters*, 896(2), L24. <https://doi.org/10.3847/2041-8213/ab982f>
- Dunn, P. A. (2023). MAVEN insitu key parameters data bundle [Dataset]. NASA Planetary Data System. Retrieved from <https://pds-ppi.igpp.ucla.edu/search/view/?f=yes&id=pds://PPI/maven.insitu.calibrated>
- Duru, F., Gurnett, D. A., Morgan, D. D., Winningham, J. D., Frahm, R. A., & Nagy, A. F. (2011). Nightside ionosphere of Mars studied with local electron densities: A general overview and electron density depressions. *Journal of Geophysical Research*, 116(A10), A10316. <https://doi.org/10.1029/2011JA016835>
- Ergun, R. E., Andersson, L., Peterson, W. K., Brain, D., Delory, G. T., Mitchell, D. L., et al. (2006). Role of plasma waves in Mars' atmospheric loss. *Geophysical Research Letters*, 33(14), L14103. <https://doi.org/10.1029/2006GL025785>
- Espley, J. R., Cloutier, P. A., Brain, D. A., Crider, D. H., & Acuña, M. H. (2004). Observations of low-frequency magnetic oscillations in the Martian magnetosheath, magnetic pileup region, and tail. *Journal of Geophysical Research (Space Physics)*, 109(A7), A07213. <https://doi.org/10.1029/2003JA010193>
- Fowler, C. M., Andersson, L., Ergun, R. E., Harada, Y., Hara, T., Collinson, G., et al. (2018). MAVEN observations of solar wind-driven magnetosonic waves heating the Martian dayside ionosphere. *Journal of Geophysical Research (Space Physics)*, 123(5), 4129–4149. <https://doi.org/10.1029/2018JA025208>
- Frahm, R. A., Sharber, J. R., Winningham, J. D., Wurz, P., Liemohn, M. W., Kallio, E., et al. (2006). Locations of atmospheric photoelectron energy peaks within the Mars environment. *Space Science Reviews*, 126(1–4), 389–402. <https://doi.org/10.1007/s11214-006-9119-5>
- Gao, J. W., Rong, Z. J., Klinger, L., Li, X. Z., Liu, D., & Wei, Y. (2021). A spherical harmonic Martian crustal magnetic field model combining data sets of MAVEN and MGS. *Earth and Space Science*, 8(10), e01860. <https://doi.org/10.1029/2021EA001860>
- Gao, Z., Su, Z., Xiao, F., Summers, D., Liu, N., Zheng, H., et al. (2018). Nonlinear coupling between whistler-mode chorus and electron cyclotron harmonic waves in the magnetosphere. *Geophysical Research Letters*, 45(23), 12685–12693. <https://doi.org/10.1029/2018GL080635>
- Gronoff, G., Arras, P., Baraka, S., Bell, J. M., Cessateur, G., Cohen, O., et al. (2020). Atmospheric escape processes and planetary atmospheric evolution. *Journal of Geophysical Research*, 125(8), e27639. <https://doi.org/10.1029/2019JA027639>
- Gurnett, D. A., Morgan, D. D., Duru, F., Akalin, F., Winningham, J. D., Frahm, R. A., et al. (2010). Large density fluctuations in the Martian ionosphere as observed by the Mars Express radar sounder. *Icarus*, 206(1), 83–94. <https://doi.org/10.1016/j.icarus.2009.02.019>

- Harada, Y., Andersson, L., Fowler, C. M., Mitchell, D. L., Halekas, J. S., Mazelle, C., et al. (2016). MAVEN observations of electron-induced whistler mode waves in the Martian magnetosphere. *Journal of Geophysical Research*, *121*(10), 9717–9731. <https://doi.org/10.1002/2016JA023194>
- Helliwell, R. A. (1969). Low-frequency waves in the magnetosphere. *Reviews of Geophysics and Space Physics*, *7*(1–2), 281–303. <https://doi.org/10.1029/RG007i001p00281>
- Helliwell, R. A. (2014). *Whistlers and related ionospheric phenomena*. Courier Corporation.
- Horne, R. B., Kersten, T., Glauert, S. A., Meredith, N. P., Boscher, D., Sicard-Piet, A., et al. (2013). A new diffusion matrix for whistler mode chorus waves. *Journal of Geophysical Research (Space Physics)*, *118*(10), 6302–6318. <https://doi.org/10.1002/jgra.50594>
- Horne, R. B., Thorne, R. M., Meredith, N. P., & Anderson, R. R. (2003). Diffuse auroral electron scattering by electron cyclotron harmonic and whistler mode waves during an isolated substorm. *Journal of Geophysical Research*, *108*(A7), 1290. <https://doi.org/10.1029/2002JA009736>
- Jakosky, B. M., Lin, R. P., Grebowsky, J. M., Luhmann, J. G., Mitchell, D. F., Beutelschies, G., et al. (2015). The Mars atmosphere and volatile evolution (MAVEN) mission. *Space Science Reviews*, *195*(1–4), 3–48. <https://doi.org/10.1007/s11214-015-0139-x>
- Jarvinen, R., Alho, M., Kallio, E., Pulkkinen, I., & Tuija (2020). Oxygen ion escape from Venus is modulated by ultra-low frequency waves. *Geophysical Research Letters*, *47*(11), e87462. <https://doi.org/10.1029/2020GL087462>
- Jin, Y., Liu, N., Su, Z., Zheng, H., Wang, Y., & Wang, S. (2022). Immediate impact of solar wind dynamic pressure pulses on whistler-mode chorus waves in the inner magnetosphere. *Geophysical Research Letters*, *49*(5), e2022GL097941. <https://doi.org/10.1029/2022GL097941>
- Katoh, Y., & Omura, Y. (2013). Effect of the background magnetic field inhomogeneity on generation processes of whistler-mode chorus and broadband hiss-like emissions. *Journal of Geophysical Research*, *118*(7), 4189–4198. <https://doi.org/10.1002/jgra.50395>
- Kennel, C. F., & Petschek, H. E. (1966). Limit on stably trapped particle fluxes. *Journal of Geophysical Research*, *71*, 1–28. <https://doi.org/10.1029/JZ071i001p00001>
- Krymskii, A. M., Breus, T. K., Ness, N. F., Hinson, D. P., & Bojkov, D. I. (2003). Effect of crustal magnetic fields on the near terminator ionosphere at Mars: Comparison of in situ magnetic field measurements with the data of radio science experiments on board Mars Global Surveyor. *Journal of Geophysical Research*, *108*(A12), 1431. <https://doi.org/10.1029/2002JA009662>
- LeDocq, M. J., Gurnett, D. A., & Hospodarsky, G. B. (1998). Chorus source locations from VLF Poynting flux measurements with the Polar spacecraft. *Geophysical Research Letters*, *25*(21), 4063–4066. <https://doi.org/10.1029/1998GL900071>
- Li, W., Thorne, R. M., Angelopoulos, V., Bortnik, J., Cully, C. M., Ni, B., et al. (2009). Global distribution of whistler-mode chorus waves observed on the THEMIS spacecraft. *Geophysical Research Letters*, *36*(9), L09104. <https://doi.org/10.1029/2009GL037595>
- Lillis, R. J., & Fang, X. (2015). Electron impact ionization in the Martian atmosphere: Interplay between scattering and crustal magnetic field effects. *Journal of Geophysical Research (Planets)*, *120*(7), 1332–1345. <https://doi.org/10.1002/2015JE004841>
- Liu, N., Su, Z., Zheng, H., Wang, Y., & Wang, S. (2018a). Magnetosonic harmonic falling and rising frequency emissions potentially generated by nonlinear wave-wave interactions in the Van Allen radiation belts. *Geophysical Research Letters*, *45*(16), 7985–7995. <https://doi.org/10.1029/2018GL079232>
- Liu, N., Su, Z., Zheng, H., Wang, Y., & Wang, S. (2018b). Prompt disappearance and emergence of radiation belt magnetosonic waves induced by solar wind dynamic pressure variations. *Geophysical Research Letters*, *45*(2), 585–594. <https://doi.org/10.1002/2017GL076382>
- Mantas, G. P., & Hanson, W. B. (1979). Photoelectron fluxes in the Martian ionosphere. *Journal of Geophysical Research*, *84*(A2), 369–386. <https://doi.org/10.1029/JA084iA02p00369>
- Meredith, N. P., Horne, R. B., & Anderson, R. R. (2001). Substorm dependence of chorus amplitudes: Implications for the acceleration of electrons to relativistic energies. *Journal of Geophysical Research*, *106*(A7), 13165–13178. <https://doi.org/10.1029/2000JA900156>
- Mitchell, D. L. (2023). MAVEN SWEA calibrated data bundle [Dataset]. NASA Planetary Data System. <https://doi.org/10.17189/1414181>
- Mitchell, D. L., Mazelle, C., Sauvaud, J. A., Thocaven, J. J., Rouzaud, J., Fedorov, A., et al. (2016). The MAVEN solar wind electron analyzer. *Space Science Reviews*, *200*(1–4), 495–528. <https://doi.org/10.1007/s11214-015-0232-1>
- NASA Planetary Data System. (2023). The Mars atmosphere and volatile evolution (MAVEN) mission data [Dataset]. https://pds-ppi.igpp.ucla.edu/search/?t=Mars&sc=MAVEN&facet=SPACECRAFT_NAME&depth=1
- Newell, P. T., Sotirelis, T., & Wing, S. (2009). Diffuse, monoenergetic, and broadband aurora: The global precipitation budget. *Journal of Geophysical Research*, *114*(A9), A09207. <https://doi.org/10.1029/2009JA014326>
- Ni, B., Thorne, R. M., Shprits, Y. Y., & Bortnik, J. (2008). Resonant scattering of plasma sheet electrons by whistler-mode chorus: Contribution to diffuse auroral precipitation. *Geophysical Research Letters*, *35*(11), L11106. <https://doi.org/10.1029/2008GL034032>
- Omura, Y. (2021). Nonlinear wave growth theory of whistler-mode chorus and hiss emissions in the magnetosphere. *Earth Planets and Space*, *73*(1), 95. <https://doi.org/10.1186/s40623-021-01380-w>
- Omura, Y., Katoh, Y., & Summers, D. (2008). Theory and simulation of the generation of whistler-mode chorus. *Journal of Geophysical Research*, *113*(A4), A04223. <https://doi.org/10.1029/2007JA012622>
- Owen, J. E. (2019). Atmospheric escape and the evolution of close-in exoplanets. *Annual Review of Earth and Planetary Sciences*, *47*(1), 67–90. <https://doi.org/10.1146/annurev-earth-053018-060246>
- Santolík, O., Gurnett, D. A., Pickett, J. S., Parrot, M., & Cornilleau-Wehrlin, N. (2004). A microscopic and nanoscopic view of storm-time chorus on 31 March 2001. *Geophysical Research Letters*, *31*(2), L02801. <https://doi.org/10.1029/2003GL018757>
- Santolík, O., Kletzing, C., Kurth, W., Hospodarsky, G., & Bounds, S. (2014). Fine structure of large-amplitude chorus wave packets. *Geophysical Research Letters*, *41*(2), 293–299. <https://doi.org/10.1002/2013GL058889>
- Seki, K., Elphic, R. C., Hirahara, M., Terasawa, T., & Mukai, T. (2001). On atmospheric loss of oxygen ions from Earth through magnetospheric processes. *Science*, *291*(5510), 1939–1941. <https://doi.org/10.1126/science.1058913>
- Shane, A., & Liemohn, M. (2021). Whistler wave interactions with superthermal electrons on martian crustal magnetic fields: Bounce-averaged diffusion coefficients and time scales. *Journal of Geophysical Research (Space Physics)*, *126*(6), e29118. <https://doi.org/10.1029/2021JA029118>
- Shane, A. D., & Liemohn, M. W. (2022). Modeling wave-particle interactions with photoelectrons on the dayside crustal fields of Mars. *Geophysical Research Letters*, *49*(2), e96941. <https://doi.org/10.1029/2021GL096941>
- Strangeway, R. J., Ergun, R. E., Su, Y. J., Carlson, C. W., & Elphic, R. C. (2005). Factors controlling ionospheric outflows as observed at intermediate altitudes. *Journal of Geophysical Research*, *110*(A3), A03221. <https://doi.org/10.1029/2004JA010829>
- Su, Z., Liu, N., Gao, Z., Wang, B., Zheng, H., Wang, Y., & Wang, S. (2020). Rapid Landau heating of Martian topside ionospheric electrons by large-amplitude magnetosonic waves. *Geophysical Research Letters*, *47*(20), e90190. <https://doi.org/10.1029/2020GL090190>
- Su, Z., Liu, N., Zheng, H., Wang, Y., & Wang, S. (2018). Large-amplitude extremely low frequency hiss waves in plasmaspheric plumes. *Geophysical Research Letters*, *45*(2), 565–577. <https://doi.org/10.1002/2017GL076754>
- Su, Z., Zhu, H., Xiao, F., Zheng, H., Wang, Y., He, Z., et al. (2014). Intense duskside lower band chorus waves observed by Van Allen Probes: Generation and potential acceleration effect on radiation belt electrons. *Journal of Geophysical Research (Space Physics)*, *119*(6), 4266–4273. <https://doi.org/10.1002/2014JA019919>

- Summers, D., Ni, B., & Meredith, N. P. (2007a). Timescales for radiation belt electron acceleration and loss due to resonant wave-particle interactions: 1. Theory. *Journal of Geophysical Research*, *112*(A4), A04206. <https://doi.org/10.1029/2006JA011801>
- Summers, D., Ni, B., & Meredith, N. P. (2007b). Timescales for radiation belt electron acceleration and loss due to resonant wave-particle interactions: 2. Evaluation for VLF chorus, ELF hiss, and electromagnetic ion cyclotron waves. *Journal of Geophysical Research*, *112*(A4), A04207. <https://doi.org/10.1029/2006JA011993>
- Teng, S., Tao, X., Li, W., Qi, Y., Gao, X., Dai, L., et al. (2018). A statistical study of the spatial distribution and source-region size of chorus waves using Van Allen Probes data. *Annales Geophysicae*, *36*(3), 867–878. <https://doi.org/10.5194/angeo-36-867-2018>
- Teng, S., Wu, Y., Harada, Y., Bortnik, J., Zonca, F., Chen, L., & Tao, X. (2023). Whistler-mode chorus waves at Mars. *Nature Communications*, *14*(1), 3142. <https://doi.org/10.1038/s41467-023-38776-z>
- Thorne, R. M., Ni, B., Tao, X., Horne, R. B., & Meredith, N. P. (2010). Scattering by chorus waves as the dominant cause of diffuse auroral precipitation. *Nature*, *467*(7318), 943–946. <https://doi.org/10.1038/nature09467>
- Tian, F. (2015). Atmospheric escape from solar system terrestrial planets and exoplanets. *Annual Review of Earth and Planetary Sciences*, *43*(1), 459–476. <https://doi.org/10.1146/annurev-earth-060313-054834>
- Tsurutani, B. T., & Smith, E. J. (1977). Two types of magnetospheric ELF chorus and their substorm dependences. *Journal of Geophysical Research*, *82*(32), 5112–5128. <https://doi.org/10.1029/JA082i032p05112>
- Wu, X., Nagano, I., Bao, Z., & Shimbo, T. (1996). Numerical simulation of the penetration and reflection of a whistler beam incident on the lower ionosphere at very low latitude. *Journal of Atmospheric and Terrestrial Physics*, *58*(10), 1143–1159. [https://doi.org/10.1016/0021-9169\(95\)00060-7](https://doi.org/10.1016/0021-9169(95)00060-7)
- Xiao, F. (2006). Modelling energetic particles by a relativistic kappa-loss-cone distribution function in plasmas. *Plasma Physics and Controlled Fusion*, *48*(2), 203–213. <https://doi.org/10.1088/0741-3335/48/2/003>
- Xiao, F., Thorne, R. M., & Summers, D. (1998). Instability of electromagnetic R-mode waves in a relativistic plasma. *Physics of Plasmas*, *5*(7), 2489–2497. <https://doi.org/10.1063/1.872932>
- Xu, S., Mitchell, D., Liemohn, M., Fang, X., Ma, Y., Luhmann, J., et al. (2017). Martian low-altitude magnetic topology deduced from MAVEN/SWEA observations. *Journal of Geophysical Research (Space Physics)*, *122*(2), 1831–1852. <https://doi.org/10.1002/2016JA023467>